NASA Technical Memorandum 83071

Analogy Between Fluid Cavitation and Fracture Mechanics

R. C. Hendricks
Lewis Research Center
Cleveland, Ohio

and

R. L. Mullen
Case Western Reserve University
Cleveland, Ohio

and

M. J. Braun
University of Akron
Akron, Ohio

Prepared for the
Thermal Engineering Joint Conference
cosponsored by the American Society of Mechanical Engineers
and the Japan Society of Mechanical Engineers
Honolulu, Hawaii, March 20–24, 1983

NASA

ANALOGY BETWEEN FLUID CAVITATION AND FRACTURE MECHANICS

R. C. Hendricks
National Aeronautics and Space Administration
Lewis Research Center
Cleveland, Ohio 44135

and

R. L. Mullen
Case Western Reserve University
Cleveland, Ohio 44106

and

M. J. Braun
University of Akron
Akron, Ohio 44325

ABSTRACT

When the stresses imposed on a fluid are sufficiently large, rupture or cavitation can occur. Such conditions can exist in many two-phase flow applications, such as the choked flows, which can occur in seals and bearings.

Nonspherical bubbles with large aspect ratios have been observed in fluids under rapid acceleration and high shear fields. These bubbles are geometrically similar to fracture surface patterns (Griffith crack model) existing in solids. Analogies between crack growth in solid and fluid cavitation are proposed and supported by analysis and observation (photographs). Healing phenomena (void condensation), well accepted in fluid mechanics, have been observed in some polymers and hypothesized in solid mechanics. By drawing on the strengths of the theories of solid mechanics and cavitation, a more complete unified theory can be developed.

E-1519

NOMENCLATURE

A	area
b_1, b_4	constants, eq. (23)
C	constant, eq. (13)
c	crack length
D	diameter
E	modulus of elasticity
E_1	slip ratio parameter
e	slip ratio parameter, eq. (31)
F	applied load
f	function, eq. (12)
f_1	function, eq. (21)
Δf	free energy, eq. (8)
G_r	reduced mass flux
G^*	flow-normalizing parameter
h	constant, eq. (8)

K	isothermal bulk modulus
k	Boltzman constant
k_1	singular point
N	number of molecules
n	exponent, eq. (13)
P	pressure
p	exponent, eq. (21)
q	exponent, eq. (26)
r	coordinate
r^*	critical size
T	temperature
$Tr(\ )$	trace
t	time
U	velocity
u_∞	free-stream velocity
V	volume
W_e	stored free energy
W_s	surface free energy
x,y	components of z
z	complex variable

Greek:

α	wedge opening angle
β	parameter, eq. (12)
δ	displacement
γ	surface energy density
$\underline{\lambda}$	modified exponent, eq. (23)
λ	bubble column wavelength
σ	stress
θ	wedge angle coordinate change
φ	stress function
ρ	density
ζ	complex variable
ν,ξ	components of ζ

Subscripts:

b	bubble
back	applied backpressure
c	thermodynamic critical
e	exit
max	maximum
rr	radial
$\theta\theta$	circumferential
$r\theta$	$r - \theta$ shear
v	vapor
0	stagnation

INTRODUCTION

Perhaps the origin of materials fracture research dates to the ancient philosophers and their quest for a harmonious universe, but the roots of modern materials fracture research appear to stem from the works of Griffith (1920) ,reference 1, on fracture of brittle materials and Berthelot (1850), reference 2, on tensile stresses of fluids. In both cases, the macroscopic approach is founded on the thermodynamics of Gibbs, Maxwell, et al., and the condition of fracture propagation depends on small displacements from a minimal energy state (i.e., a metastable state). Although sharing this fundamental base, the fields of fluid and solid fracture have developed into disjoint areas of research. Some early work on the relations of fluids and crystals, including the formation of voids and dislocations (fracture), is accumulated in the text by Frenkel (ref. 3). From these areas entire fields have developed, namely, two-phase flows and boiling, fracture mechanics, cavitation, metastability, etc., with texts by Tong, Hsu-Graham, Lahey, Wallis, Hewitt, et al. (refs. 4 to 8), for example, in two-phase flows and boiling; Shi, Brock, Liebowitz, and Knott (refs. 9 to 12) in fracture mechanics; Knapp, et al., and work of Acosta, Briggs, Floberg, Temperley, etc. (refs. 13 to 17) in cavitation; Skripov and work by Leinhard, etc. (refs. 18 and 19) in metastability - to cite only a few.

The problems in fluid and solid fracture are further complicated when thin films are involved, such as in tribology (e.g., see the Leeds-Lyon Conference Series, ref. 20, and monolayer development (e.g., Etters, ref. 21)). Still more complications are added when two-phase flows and heat transfer with and without sliding contact are considered (refs. 22 to 26). In most of these cases the flow-imposed stresses are sufficiently large to fracture (cavitate) the fluid. Such conditions can be readily developed in such applications as two-phase choked flows, seals, and bearings (refs. 22 to 30).

In this paper the Fisher-Frenkel and Griffith models for fracture propagation in fluids and solids are briefly reviewed, and the parallel nature of theoretical solutions involving wedge-shaped boundaries and observed fracture and cavitation patterns for fluids and solids are discussed. Finally, by integrating these results, a unified approach is proposed to describe a sequence of events associated with the passage of a large bubble through a narrow channel in two-phase, radially inward flow of fluid nitrogen.

ANALOGY BETWEEN GRIFFITH AND FISHER-FRENKEL CRACK MODELS

For both models, one postulates that a crack will grow or propagate whenever the incremental release of reversible, stored free energy W_e

$$dW_e = F\, d\delta \tag{1}$$

becomes larger than the incremental release of surface free energy W_s

$$dW_s = \gamma\, dA \tag{2}$$

caused by the formation of a new surface. Here F is the applied load, δ the displacement, A the surface area, and γ the surface energy density.

Fisher-Frenkel Crack Model (refs. 3 and 31)

The reversible work of formation for a spherical volume V (analogous to gas spring) is

$$dW_e = F\, d\delta = Tr(\sigma)dV = 4\pi r^2 \sigma\, dr \tag{3}$$

where $Tr(\sigma)$ is the negative of the applied pressure ($Tr(\sigma) = -P$). The release of surface energy, which is related to the cohesive energy and latent heat of vaporization, for an expanding sphere is

$$dW_s = \gamma\, dA = 8\pi\gamma r\, dr \tag{4}$$

The total energy change at equilibrium becomes

$$dW = dW_e - dW_s \tag{5}$$

and the critical radius becomes

$$r^* = \frac{2\gamma}{\sigma} = -\frac{2\gamma}{\Delta P} \tag{6}$$

where ΔP is the difference outside and inside pressures of the volume V. Perhaps the most critical comment is that the theory only considers the systems which will grow isotropically. The rates (inertial, viscous) and the influence of nearest neighbors in attempting to propagate or to 'heal' the crack (inhomogeneity or void collapse) are also ignored.

For a favorable chain of statistical events (pressure and thermal fluctuations) such that $r > r^*$, the total energy becomes

$$W = -16\pi\gamma^3/3[Tr(\sigma)]^2 \tag{7}$$

For a volume generation rate and a rate constant both related to first-order reactions (Arrhenius functions), Fisher (ref. 31) gives

$$Tr(\sigma) = -P = \left[\frac{16\pi}{3}\left(\frac{\gamma^3}{kT\ \ln(NKTt/h) - \Delta f}\right)\right]^{1/2} \tag{8}$$

where $-P$ denotes tensile stress; for water $Tr(\sigma)$ is about 130 MPa (ref. 31), which is about an order of magnitude too high (refs. 13, 17, and 31) for pure water in a clean experimental apparatus, two orders for water on regular surfaces, and three orders for gassed water on irregular surfaces. Temperley (ref. 17) gives 3 to 5 MPa for water on glass.

In the appendix, we show that a change in parameters leads to a form for r^* which is nearly the same as that derived for the Griffith model discussed in the next section.

Griffith Crack Model (ref. 1)

The incremental reversible work of formation, for two surfaces of a disk-shaped crack, is represented by

$$dW_e = \frac{2\pi[Tr(\sigma)]^2}{E} c^2 \, dc \tag{9}$$

where F is the applied load, $2c$ is the crack length, $Tr(\sigma)$ is the stress, and E is Young's modulus (proportional to isothermal bulk modulus). The surface energy γ is proportional to the cohesive energy and latent heat of sublimation,

$$dW_s = \gamma \, dA = 4\pi\gamma c \, dc \tag{10}$$

At equilibrium, the critical crack radius becomes

$$c^* = 2\gamma E/\pi[Tr(\sigma)]^2 \tag{11}$$

and again if $c > c^*$, the crack will grow; otherwise the disturbance will decay. Calculations using this relation give stresses up to two orders of magnitude greater than observed (ref. 32).

The estimated fracture stresses for both models are too large. We postulate that strained nuclei communicate at a wave speed dependent on the propagation and echo return rates. When sufficient energy is available, the nuclei can connect in accordance with nearest-neighbor principles. These connections form cracks or voids. The point is that the maximum stress prior to cracking is highly dependent on the environment, because small fluctuations in the geometry or the material properties may decrease the required free energy. Experimentalists in boiling, cavitation, two-phase and choked two-phase flows, and fracture mechanics create artifical sites, sharp changes in streamlines, and high gradients or notches which may be classified as artificial cracks in order to 'capture' the phenomena for study. This is not wrong , but it does alter the surface free energy in such a way that the boundaries constitute the source for the fracture propagation. And indeed in reality, fractures usually originate at the free boundary as modeled. Thus, the analyses which ignore small fluctuations serve as guides for experiment because the actual measured values will be less. Perhaps a practical limit would be $Tr(\sigma)_{calc}/100$.

SINGULARITIES OF CRACK TIP AND WEDGE FLOWS

The uniqueness of solutions to the conventional field equations of solid and fluid mechanics has been shown for most boundary conditions (Teman, ref. 33, fluid, and Wheeler, ref. 34, solid). One of the conditions required for uniqueness is that the domain of the problem satisfy some form of a Lipshitz condition. When the domain of the problem contains a wedge-shaped region, the Lipshitz condition is not satisfied. Therefore multiple solutions can be obtained.

As an example of this phenomenon, a generalization of the Williams solution (ref. 35) of a slit in an elastic solid and the Falkner-Skan solution

for flow over a wedge will be compared. In both problems the domain considered is an unbounded region with a wedge. We will later relate these results to fracture photographs (solid and fluid) and radially inward flow sequences for fluids.

Wedge Flow Solution

Let us assume that a bubble in radially inward flow can be transformed (elongated) to appear as a Zhukovskii (Joukowsky) airfoil (ref. 36) (fig. 1). Here the circle passes through the singular point (-k) and the trailing-edge curvature is not continuous. Without the attendant Kutta condition, separation and flow reversal can occur at any angle of attack. Critical here is the radius of curvature of an element's trajectory (sharpness of the edge), which determines the associated stress field. Further, let us assume that the flow can then be directed at the trailing edge as for flow over a wedge (fig. 2(a)). The problem can be solved by means of the Falkner-Skan equation applied to a limited portion on the trailing edge of the bubble.

$$f''' + ff'' + \beta(1 - f'^2) = 0 \tag{12}$$

where $\beta = 2\alpha/\pi$. The free-stream velocity will vary as

$$u_\infty = Cr^n \tag{13}$$

$$n = \alpha/(\pi - \alpha) \tag{14}$$

and the pressure will be obtained from

$$u_\infty \, du_\infty/dr = -dP/dr \tag{15}$$

as

$$-dP/dr = Cnr^{2n-1} \tag{16}$$

and

$$P = -Cnr^{2n}/2n + P_0 \tag{17}$$

Separation in this case will occur when

$\beta = -0.1988 \rightarrow \alpha = -0.312$ rad

and consequently

$n = -0.09$

Cavitation will accompany the separation process if the characteristics of the free flow will permit the pressure around the wedge tip to fall below the liquid vapor pressure. The physical significance of the negative β

can be better understood if an equivalent positive angle is substituted. This underscores the fact that the solution of the flow equations is not unique until the power n is specified; with n specified, the power of the singularity of r^{2n} in the pressure is established and the resulting pressure field becomes unique.

Elasticity Solution

For the region shown in figure 2(b), the boundary conditions are

$$\begin{aligned} &r > 0 \qquad \theta = \pm(\pi - \alpha) \qquad \sigma_{\theta\theta} = \sigma_{\theta r} = 0 \\ &r \to \infty \qquad\qquad\qquad\quad \sigma_{r\theta} = \sigma_{rr} = 0 \end{aligned} \tag{18}$$

If we define a stress function φ such that

$$\sigma_{rr} = \frac{1}{r^2}\frac{\partial^2\varphi}{\partial\theta^2} + \frac{1}{r}\frac{\partial\varphi}{\partial r};\quad \sigma_{\theta\theta} = \frac{\partial^2\varphi}{\partial r^2};\quad \sigma_{r\theta} = \frac{1}{r^2}\frac{\partial\varphi}{\partial\theta} - \frac{1}{r}\frac{\partial^2\varphi}{\partial r\,\partial\theta} \tag{19}$$

the stress always satisfies the equilibrium equations; also, the compatibility equations reduce to

$$\nabla^4\varphi = 0 \tag{20}$$

If one assumes a stress function in the form

$$\varphi = r^p f_1(\theta) \tag{21}$$

where $f_1(\theta)$ is an arbitrary function of θ, the compatibility equation will yield the following ordinary differential equation for the function f_1:

$$f_1^{iv} + \left[p^2 + (p-2)^2\right]f_1'' + \left[p^2(p-2)^2\right]f_1 = 0 \tag{22}$$

This linear ordinary differential equation has four terms in its homogeneous solution; the function f_1 is then given by

$$f_1(\theta) = b_1 \sin(\lambda+1)\theta + b_2 \cos(\lambda+1)\theta + b_3 \sin(\lambda-1)\theta + b_4 \cos(\lambda-1)\theta \tag{23}$$

where

$$\lambda = 1 - p \tag{24}$$

By splitting the problem into symmetric and antisymmetric stress fields and enforcing the boundary conditions (eq. (17)) on the surface of the wedge, the following condition on λ is imposed:

$$(\lambda + 1)^2 \cos(\lambda - 1)(\pi - \alpha)\sin(\lambda + 1)(\pi - \alpha)$$

$$- (\lambda^2 - 1)\sin(\lambda - 1)(\pi - \alpha)\cos(\lambda + 1)(\pi - \alpha) = 0 \qquad (25)$$

Therefore the pressure at the fracture tip in both the fluid and solid can be expressed in the form

$$p \propto r^q \qquad (26)$$

where

$$q = \begin{cases} 2n & \text{fluid} \\ 1 - \frac{n}{2} & \text{solid} \end{cases}$$

A graph of q as a function of wedge angle is shown as figure 3.

Since the boundary conditions and field equations are satisfied for any $p \propto r^q$, where n is any integer, several powers of r are valid solutions to the boundary value problem. Although physical arguments can be used to eliminate some of the solutions, the classical remedy to the multiple solutions in fluid and solid mechanics was to force the power of r to match the limit of problems involving the Lipshitz admissible domain.

However, the existence of these singularities can explain the discrepancy between experimentally observed and theoretically predicted fracture strengths. These local singularities, when averaged over a measurable domain, will appear as some significantly lower value. Consequently, in the limit of the singular region the values predicted by the Griffith and Fisher-Frenkel models could be correct.

FRACTURE PHOTOGRAPHS

To further illustrate some analogies of crack propagation in solids and liquids, we have selected four photographs: two of solid fracture and two of liquid fracture.

Figure 4(a) shows a crack tip region (ref. 37) from which the crack propagates if the energy criteria equation is satisfied (i.e., stored energy > energy required to make a new surface, eqs. (1) and (2)). The crack tip is typically very pointed, and healing requires additional energy in the form of heat or stress (or both). Note that the crack tip here could be superimposed onto the previously discussed fluid crack tips (fig. 2). The healing of a fluid crack also requires additional energy; in two-phase flows the surrounding pressure field is usually sufficient. However, if the collapse of the crack is to occur without rebound or additional dynamic phenomena, addition of heat will 'soften' the impact (the heat will drive the system toward saturation in the subcritical state and in the supercritical state - supposedly only second-order phase transitions are possible). The similarity between the development of hole mobility in both solids and liquids with stress and temperature is striking, but not unexpected, as the basic concepts are virtually the same.

Figure 4(b) shows a 'feather' crack propagated in a polypropylene plastic block (ref. 38). Here one can clearly see a main-line crack with a multiplicity of smaller cracks emanating from it generally at an oblique angle of approximately 30°. The procedure is that the crack propagates to some nonhomogeneity, stops, and 'shoots' a side crack; upon building sufficient energy, the sequence is repeated. The influence of bulk voids and boundaries is significant. Irregularities as nonhomogeneities and surface scratches lower the free energy for crack propagation, which alters the developing pattern.

Figure 4(c) illustrates fluid fracture (cavitation) in a simulated journal bearing (ref. 39). There appears to be a connected set of line cracks forming the main-line crack with a series of nominal normally propagated cracks forming a fern-like structure. The cracks are assumed to form in a manner similar to the feather pattern described above. Here, surface-active sites lower the free energy requirements for cracking by serving as sources (sinks) for surface-fluid-induced cracking, while distributed nuclei lower the energy requirement for bulk-fluid-induced cracking (homogeneous).

Figure 4(d) illustrates how a thin fluid film constrained between two parallel surfaces fractures as the surfaces are pulled apart (ref. 40). The radial cracks propagate to later establish fern structure or network patterns which we have observed in our own work (see motion picture supplement).

These 'starburst' fracture patterns are also observed in radially inward flow of nearly saturated fluid nitrogen (ref. 22, fig. 11).

Further investigation into the radially inward flow data of reference 22 revealed two apparent fracture patterns, pseudo-steady as cited in figure 4(d) and dynamic fluid fracture, which are discussed in the following section.

RADIALLY INWARD FLOWS

Description of Apparatus

The apparatus is described in reference 22, but some essential features are worth outlining here. The dewar was a double-walled, high-pressure vessel with viewing ports, as illustrated in figure 5. The radially inward flow passage was formed by a glass flat and a stainless-steel orifice flat separated by three radial wires of 0.0076 cm diameter (3 mils) at 120°. The radial passage was 0.72 cm in length or approximately 133 L/D. Further details of the configuration are given in figure 5 and reference 22.

Estimates of Fluid and Bubble Velocities

For the motion picture sequences, illustrated photographically in figures 6 and 7 and schematically in figures 8 and 9, the inlet stagnation conditions (ref. 22) are P_0 = 1.5 MPa and the liquid nitrogen is saturated. Actually, there must exist a small degree of subcooling; otherwise the bubble population would be much higher. Under these conditions and for the geometry of figure 5, two-phase choked flow occurs and can be calculated by solving

$$G_r^2 = \frac{2\rho^2}{G^{*2}} \int_{P_e}^{P} \frac{d\rho}{\rho} \tag{27}$$

subject to the constraint that

$$G_{max}^2 \left(\frac{1}{\rho^2} \frac{dP}{d\rho} \right) \Bigg|_e = G^{*2} \tag{28}$$

where $G^* = \sqrt{P_c \rho_c / Z_c}$ (refs. 27-29). The effect of friction for these flows is small (to 10 percent) as compared with that of the convective terms and was therefore omitted. The solution gives the reduced mass flux as (refs. 27 and 28)

$$\begin{aligned} G_{r,max} &= 0.23 \quad \text{equilibrium} \\ G_{r,max} &= 0.33 \quad \text{nonequilibrium} \end{aligned} \tag{29}$$

Assuming that either a small degree of subcooling or metastability occurs, the average equilibrium fluid velocity for nitrogen becomes 2240 cm/sec. From figure 10, which represents the bubble traverse of figures 6 to 9, the average velocity of the bubble head is 2350 cm/sec, giving a slip velocity ratio of 1.05. The bubble head velocity near the exit orifice (fig. 5) is estimated at 4000 cm/sec; the liquid sonic velocity is 4900 cm/sec. The maximum possible slip ratio, based on inertia-dominated, stratified two-phase flows are $(\rho_\ell / \rho_v)^{1/2} = 3.1$ for $P_0 = 1.5$ MPa and 12 for $P_{back} = 0.12$ MPa.

Thus the slip ratio for the bubble head appears to be

$$\begin{aligned} 1.05 < (U_b/U_\ell)_{head} < 1.8 < \sqrt{\rho_\ell/\rho_v}_{max, P_0=1.5} = 3.1 \\ < \sqrt{\rho_\ell/\rho_v}_{P_{back}=0.12} = 12 \end{aligned} \tag{30}$$

Using the same procedure, velocity estimates can be made for the bubble tail. From figures 6 to 9 the average velocity appears to be 1200 cm/sec, while the velocity near the exit appears to have decreased to 850 cm/sec. In either case the 'slip' ratio is significantly less than 1 over most of the traverse across the channel, and this demonstrates that the bubble tail travels at a rate much less than the local fluid velocity (i.e., the fluid is impaled on the bubble tail)

$$e < (U_b/U_{tail}) < E_1 (E_1 = 1, \text{ majority of the traverse}) \tag{31}$$

A closer examination of the data of figures 6 to 9 shows that $e < 0$ is admissible. And for a bubble flowing into a developed cavity formed by a previous bubble, the tail closure rate can be well above the average fluid velocity, $E_1 > 1$. In this case, void condensation (crack healing) is not understood. Furthermore the bubble tail 'meanders,' which may be attributed to local vortex streets shed by the passing bubble, specific nucleation sites along the bubble path, and perhaps bubble column stiffness variations leading to buckling wave lengths ($\bar{\lambda}_{c_1}$) about twice those predicted (ref. 41),

$$\bar{\lambda}_1 = 2\bar{\lambda}_{c_1} = \pi D_{bubble} \tag{32}$$

Pseudo-Steady Fracture

Figure 11 is a frame taken from a 8000 pps motion picture sequence, where Po = 1.5 MPa and T → Tsat. It is essentially the one shown in ref. 22. The extreme irregularity in the two-phase interface may be viewed as pseudo-steady fluid fracture.

SUMMARY

We have discussed the similarities between the Griffith and Fisher-Frenkel crack models for solids and liquids, respectively. Both models predict stresses which are significantly greater than experiment - but by nearly the same magnitude. The values are affected principally by impurities and the presence of sharp boundaries (i.e., stress concentrators). Since the calculations are very complex, a practical estimate would be $\sigma_{calc}/100$. We postulate that nuclei can communicate by wave propagation and follow nearest-neighbor principles.

The singularity at the crack tip and that associated with wedge flows exhibit the same type of behavior, indicating that fluid cracking is indeed possible. Photographs of crack propagation in solids and cavitation in bearings and separating flat surfaces appear to possess a commonality in that the main-line crack and attached cracks have similar characteristics. Furthermore an analysis of the radially inward flow of two-phase choked flow of fluid nitrogen indicates that the bubble head traverses the narrow channel with a slip ratio greater than unity. The bubble tail travels much more slowly and the fluid impales itself on the bubble tail, which implies the existence of fluid cracking. For this case, void condensation (crack healing) is not understood.

These analyses and photographs imply the existence of solid and fluid fracture and reinforce the analogy between cavitation and fracture mechanics models. Although these models have a common basis in molecular mechanics, the fields have developed dissimilar methods and there is a need for enhanced crossflow of information.

APPENDIX - FLUID FRACTURE MODEL, A CHANGE IN PARAMETERS

Assume that the incremental decrease in stored energy due to a crack advance (change in volume) is

$$\Delta W_e = -\Delta P\ \Delta V = \frac{(\Delta P)^2\ V}{K} \tag{A1}$$

where K is the isothermal bulk modulus ($K = E/3(1 - \nu)$ for solids).

The creation of additional fracture surface requires an incremental energy

$$\Delta W_s = \gamma\ \Delta A \tag{A2}$$

and for the spherical model, the critical radius becomes

$$r^* = 2\gamma K/\Delta P^2 \quad \text{or} \quad \Delta P \sim P = \sqrt{\frac{2\gamma K}{r^*}} \tag{A3}$$

which is nearly the same as postulated for the Griffith model in solid fracture.

Following Fisher (ref. 31) the predicted value of stress becomes

$$\mathrm{Tr}(\sigma) = -P = \frac{16\pi}{3}\left[\frac{K^2\gamma^3}{kT(\ln NkTt/h) - \Delta f}\right]^{1/4} \tag{A4}$$

For water, $\mathrm{Tr}(\sigma) = 500$ MPa, which is about 100 times the 3- to 5-MPa value for water on glass recommended by Temperley (ref. 17). When the relation $\sigma = \sqrt{2\gamma E/\pi c}$ from the Griffith model is used, the predicted stresses are also about 100 times too large (ref. 33).

REFERENCES

1. Griffith, A. A., "Phemonena of Rupture and Flow in Solids," Philosophical Transactions of the Royal Society of London, Series A, Vol. 221A, 1921, pp. 163-198.

2. Bertholet, M., "Sur quelques phenomenes de dilation forcee de liquides," Annales de Chimie et de Physique, Vol. 30, 1850, p. 232.

3. Frenkel, J., Kinetic Theory of Liquids, Dover Publications, New York, 1955.

4. Tong, L. S., Boiling Heat Transfer and Two-Phase Flow, John Wiley and Sons, New York, 1965.

5. Hsu, Y. Y. and Graham, R. W., Transport Processes in Boiling and Two-Phase Systems, Hemisphere Publishing Corporation, Washington, D.C., 1976.

6. Lahey, R. T. and Moody, F. J., The Thermal Hydraulics of a Boiling Water Nuclear Reactor, American Nuclear Society, Hinsdale, Ill., 1977.

7. Wallis, G., One Dimensional Two-Phase Flow, McGraw-Hill, New York, 1969.

8. Hewitt, G. F., Delhaye, J. M., and Zuber, N., Multiphase Science and Technology, Vol. 1, Hemisphere Publishing Corporation, Washington, D.C., 1982.

9. Shi, G. C., Proceedings of an International Conference on Dynamic Crack Propagation, Noordhoff International Publ., Leyden, 1973.

10. Brock, D., Elementary Engineering Fracture Mechanics, Noordhoff International Publ., Groningen, 1974.

11. Liebowitz, H., Fracture, an Advanced Treatise, Academic Press, New York, 1968.

12. Knott, J. F., Fundamentals of Fracture Mechanics, Butterworth, London, 1973.

13. Knapp, R. T., Daily, J. W., and Hammitt, F. G., Cavitation, McGraw-Hill New York, 1970.

14. Acosta, A. J., "An Experimental Study of Cavitating Inducers," Hydrodynamic Noise, Cavity Flow, Second Symposium on Naval Hydrodynamics, ONR/ACR-38, Office of Naval Research, 1958, pp. 533-557.

15. Briggs, L. J., Limiting Negative Pressure of Water," Journal of Applied Physics, Vol. 21, No. 7, July 1950, pp. 721-722.

16. Floberg, L., "On Hydrodynamic Lubrication with Special Reference to Sub-cavity Pressures and Number of Streamers in Cavitation Regions," Acta Polytechnica Scandinavica, Mehanical Engineering Series, No. 19, 1965.

17. Temperley, H. N. V. and Chambers L. L. G., "The Behavior of Water Under Hydrostatic Tension, I and II," Proceedings of the Physical Society, London, Vol. 58, Pt. 4, July 1946, pp. 420-443.

18. Skripov, V. P., Metastable Liquids, John Wiley, New York, 1973.

19. Leinhard, J., Thermodynamics, John Wiley, New York, 1982.

20. Dowson, D., Godet, M., and Taylor, C. M., Cavitation and Related Phenomena in Lubrication, Mechanical Engineering Publications, London, 1975.

21. Etters, R. D., Pan, R., and Chandrasekharan, V., "Two-Dimensional Oxygen Absorbed on Graphite," Physical Review Letters, Vol. 45, No. 8, Aug. 1980, pp. 645-648.

22. Hendricks, R. C., Simoneau, R. J. and Hsu, Y. Y., "A Visual Study of Radial Inward Choked Flow of Liquid Nitrogen," Advances in Cryogenic Engineering, Vol. 20, Plenum Press, New York, 1975, pp. 370-382.

23. Hughes, W. F. and Beehler, R. M., "Turbulent Two-Phase Flow in Ring and Face Seals," International Conference on Fluid Sealing, 9th Noordwijkerhout, The Netherlands, 1981, pp. 185-202.

24. Lebeck, A. O., "A Mixed Friction Hydrostatic Face Seal Model with Phase Change," ASME 79-LUB-5, American Society of Mechanical Engineers, Oct. 1979.

25. Hendricks, R. C., Braun, M. J., Arp, V., and Giarrantano, P. J, "The Dryout Region in Frictionally Heated Sliding Contacts," International Heat Transfer Conference, 7th, Sept. 6-10, 1982, Munich, American Society of Mechanical Engineers.

26. Braun, M. J. and Hendricks, R. C., "An Experimental Investigation and Some Analytical Considerations Concerning Vaporous/Gaseous Cavity Characteristics of an Eccentric Shaft Seal or Bearing," Heat and Mass Transfer in Rotating Machinery, XIV International Centre for Heat and Mass Transfer, Dubrovnik, Yugoslavia, 1982.

27. Simoneau, R. J. and Hendricks, R. C., "Generalized Charts for Computation of Two-Phase Choked Flow of Simple Cryogenic Liquids," Cryogenics, Vol. 17, No. 1, Jan. 1977, pp. 73-76.

28. Simoneau, R. J. Hendricks, R. C., "Two-Phase Choked Flow of Cryogenic Fluids in Converging-Diverging Nozzles," NASA TP-1484, 1979. National Aeronautics and Space Administration, Cleveland, OH.

29. Hendricks, R. C. and Sengers, J. V., "Application of the Principle of Similarity to Fluid Mechanics," Water and Steam: Their Properties and Current Industrial Applications, Pergamon Press, Oxford, 1980.

30. Jacobsen, B. O. and Hamrock, B. J., "High-Speed Motion Picture Camera Experiments of Cavitation in Dynamically Loaded Journal Bearings," NASA TM-82789, 1982, National Aeronautics and Space Administration, Cleveland, OH.

31. Fisher, J. C., "The Fracture of Liquids," Journal of Applied Physics, Vol. 19, No. 11, Nov. 1948, pp. 1062-1067.

32. Guy, A. G., Essentials of Materials Science, McGraw-Hill, New York, 1976.

33. Teman, R, Lecture Notes - NSF/CBMS Conference on the Navier Stokes Equations and Non-linear Functional Analysis, Dekalb, Ill., Aug. 1981.

34. Wheeler, L. T. and Sternbery, E., "Some Theorems in Classical Elastohydrodynamics," Archive for Rational Mechanics and Analysis, Vol. 31, 1968, pp. 51-90.

35. Williams, M. L., "On the Stress Distribution at the Base of Stationary Crack," Journal of Applied Mechanics, Vol. 24, Mar. 1957, pp. 109-114.

36. Rauscher, M., Introduction ot Aeronautical Dyanamics, Wiley, New York, 1953.

37. Bothsis, J., Case Western Reserve University, Private Communication.

38. Moet, A., Case Western Reserve University, Private Communication.

39. Dauble, H., Daimler-Benz, A. G., and Stutgart, F. R. G., "Movable Face Seals Under Pulsating Pressure," International Conference on Fluid Sealing, 9th, Noordweijkerhout, The Netherlands, 1981, pp. 25-36.

40. Hays, D. E. and Feiten, J. B., "Cavities Between Moving Parallel Plates," Cavitation in Real Fluid, Elsevier, New York, 1964, pp. 122-137.

41. Stockman, M. G. and Bejan, A., "The Nonaxisymmetric (buckling) Flow Regime of Fast Capillary Jets," Physics of Fluids, Vol. 25, No. 9, Sept. 1982, pp. 1506-1511.

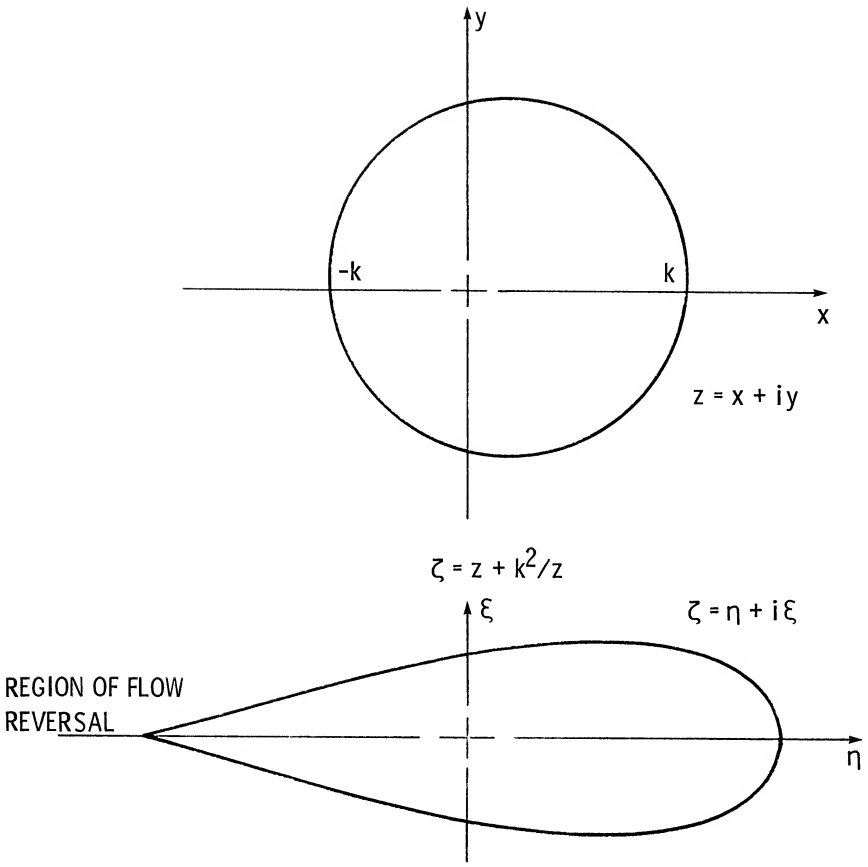

Figure 1. - Zhukovskii transformation of a cylinder to an airfoil.

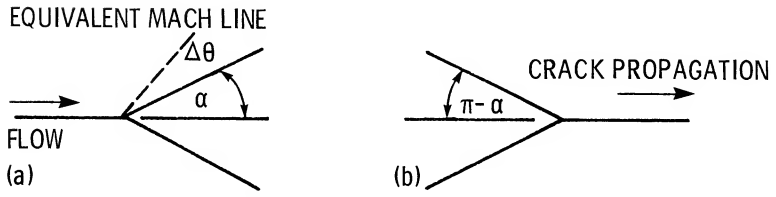

(a) Wedge flow solution.
(b) Elasticity solution.

Figure 2.-Schematic illustrating singularity regions for wedge flow and crack tip.

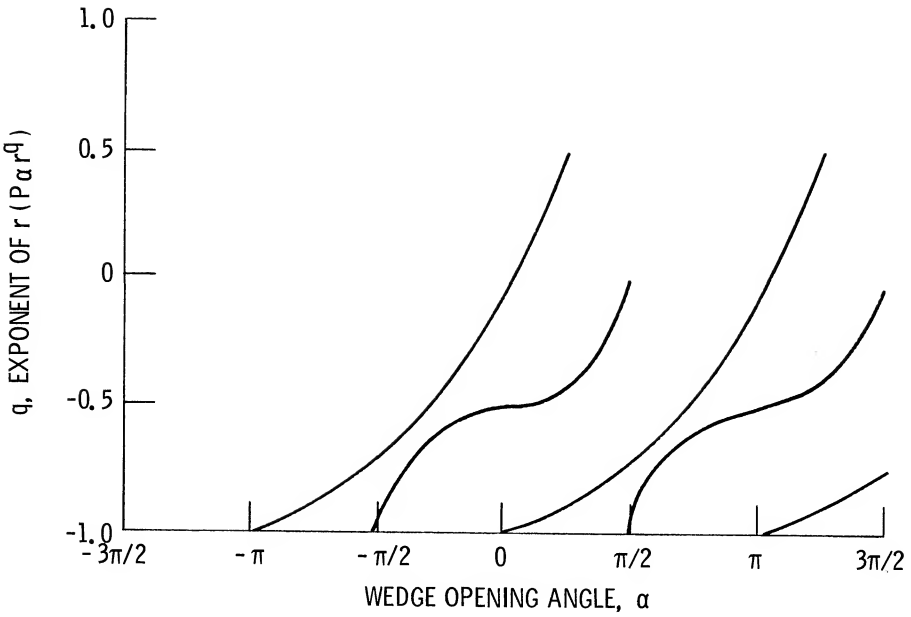

Figure 3. - Dependence of pressure on the power of r.

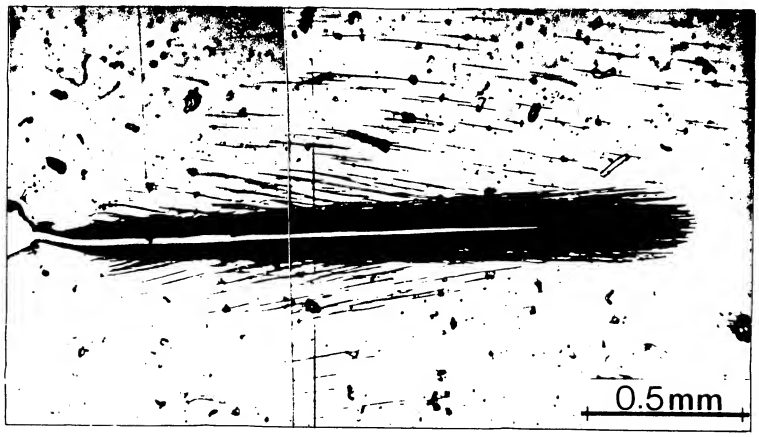

(a) Crack tip.

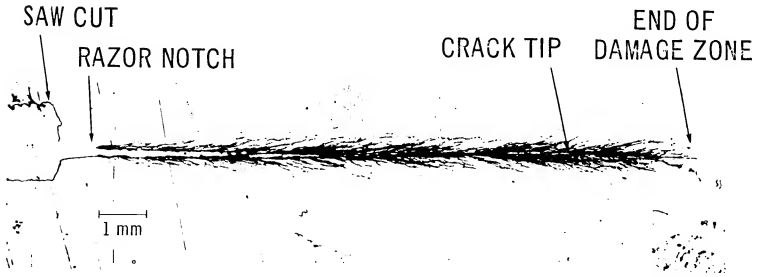

(b) Feather crack in polypropylene (plastic). Fatigue crack in 8 mm thick compact tension specimen of polypropylene. The micrograph is taken from a thin section (~ micrometer) cut normal to the fracture surface. Note the damage disseminated around and ahead of the main crack.

Figure 4. - Fracture propagation in solids and liquids.

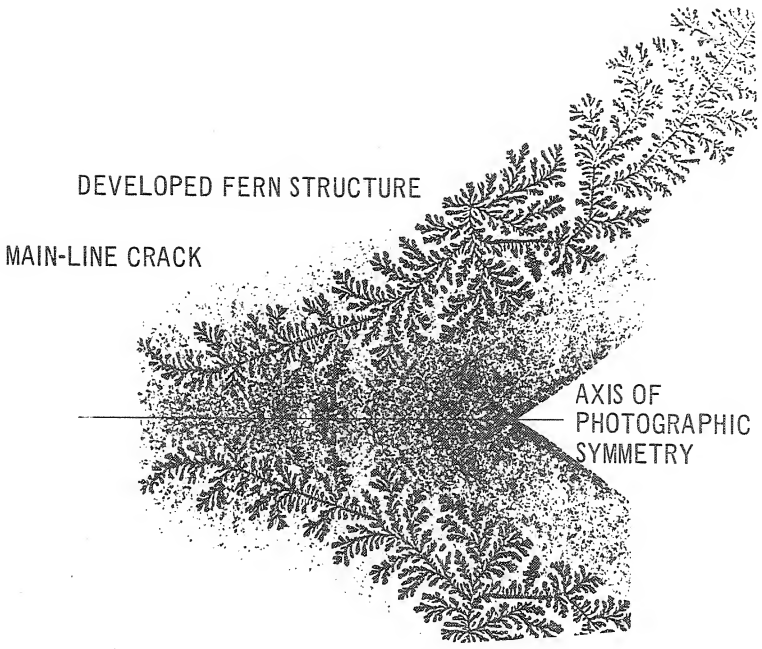

(c) Cavitation in a bearing.

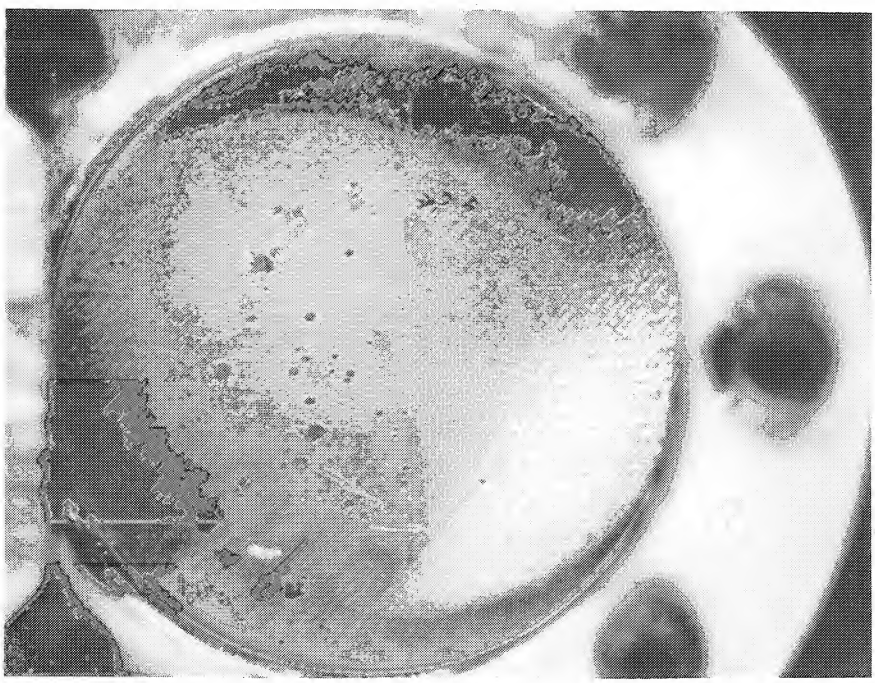

(d) Fluid fracture between parallel plates.

Figure 4. - Concluded.

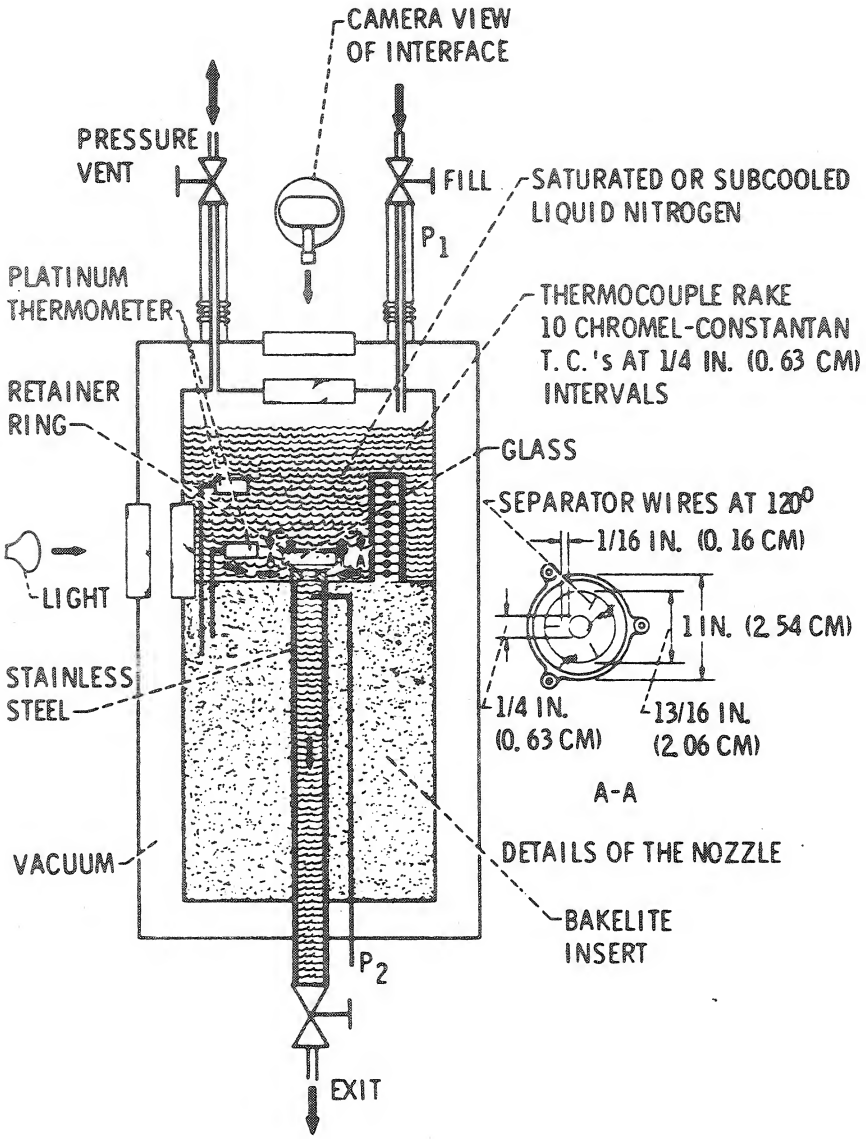

FIGURE 5. - SCHEMATIC OF RADIAL INWARD FLOW CRYOSTAT, REF. 22.

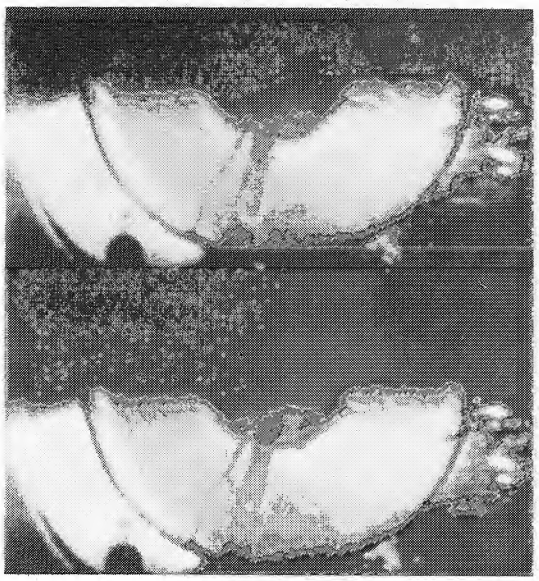

(4a) Top of frame.
(4b) Bottom of frame.

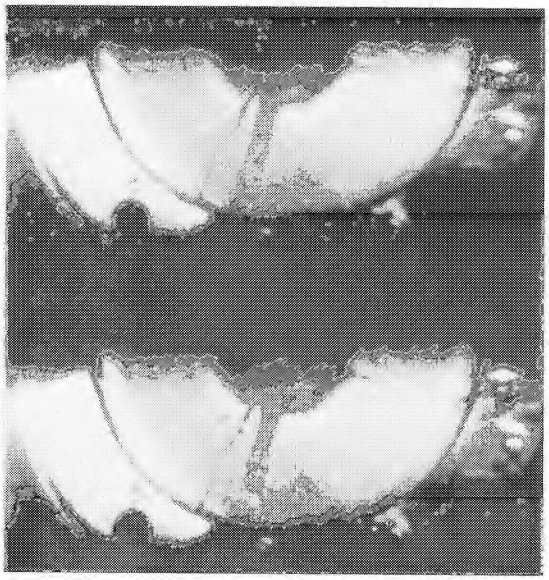

(5a) Top.
(5b) Bottom.

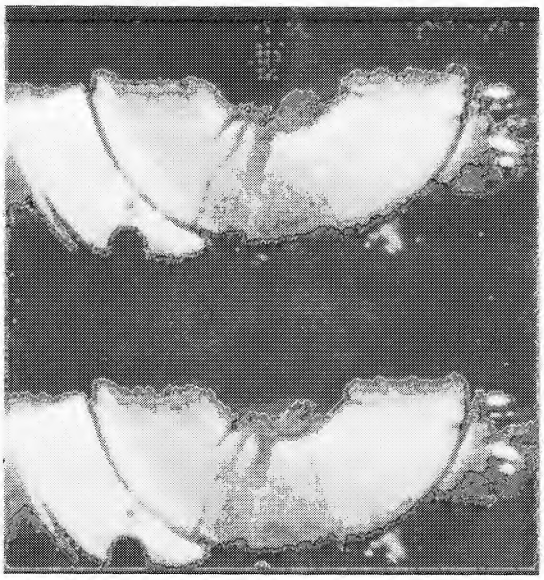

(6a) Top.
(6b) Bottom.

Figure 6. - Photographic representations of bubble traverse for radial inward flows of fluid nitrogen. Corresponding data plots shown in figure 10.

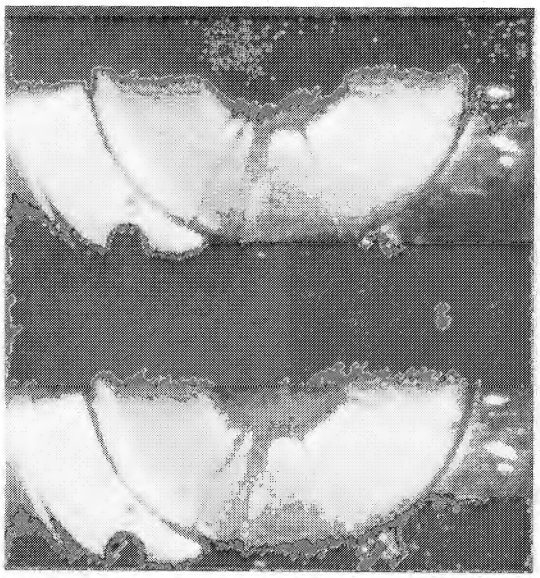

(7a) Top.
(7b) Bottom.

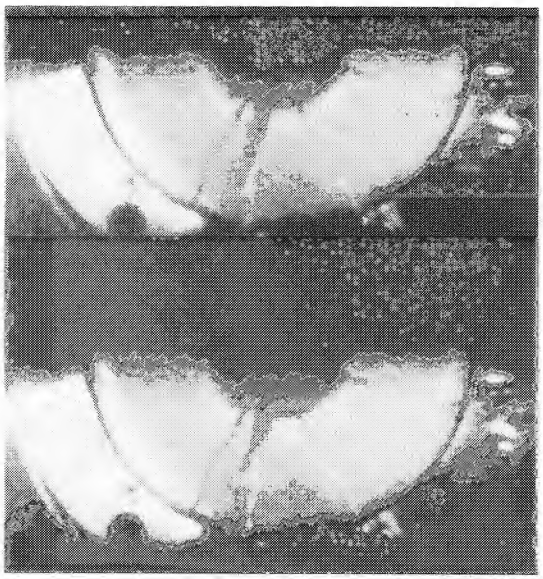

(8a) Top.
(8b) Bottom.

(9a) Top.
(9b) Bottom.

Figure 7. - Photographic representations of bubble traverse for radial inward flows of fluid nitrogen. Corresponding data plots shown in figure 10.

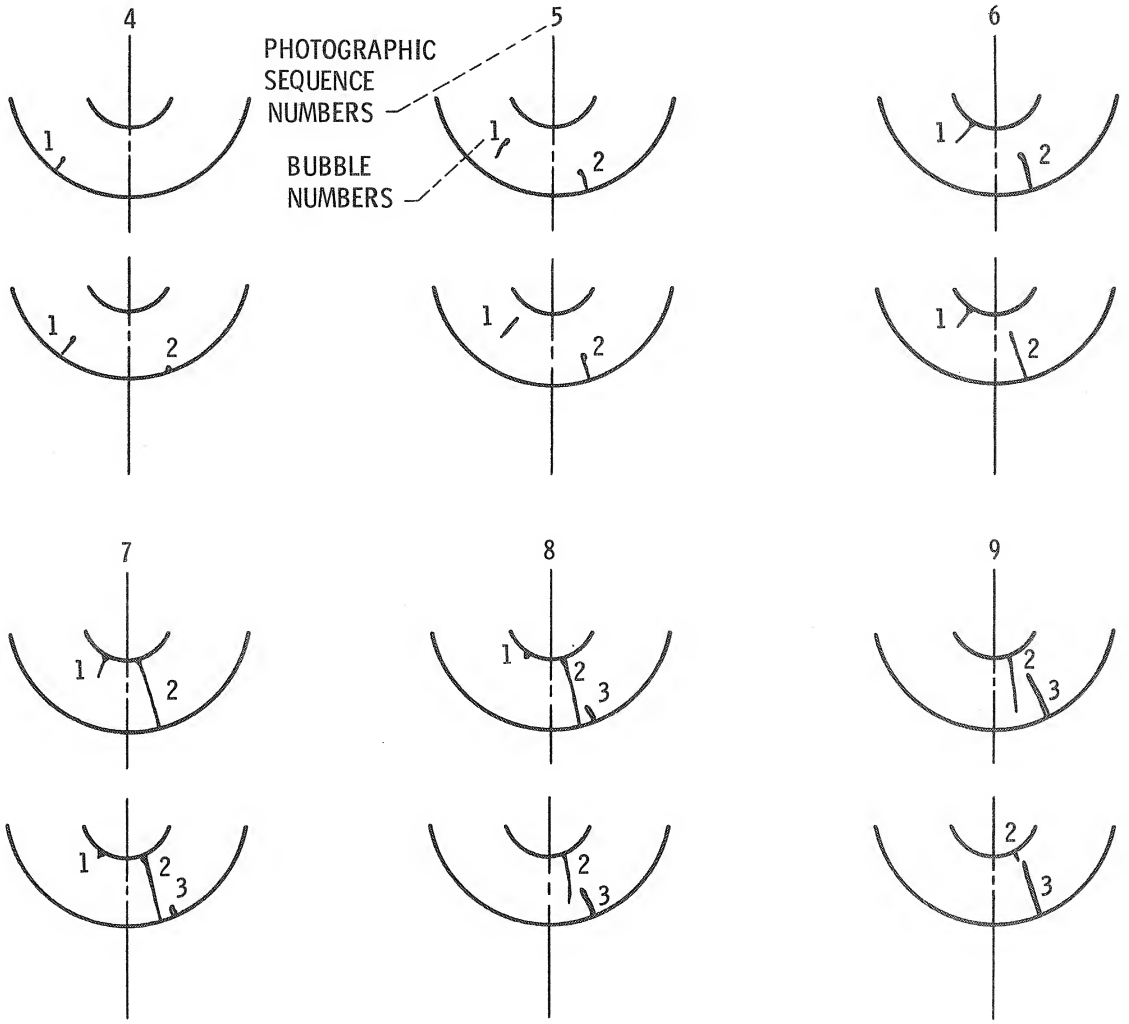

Figure 8.

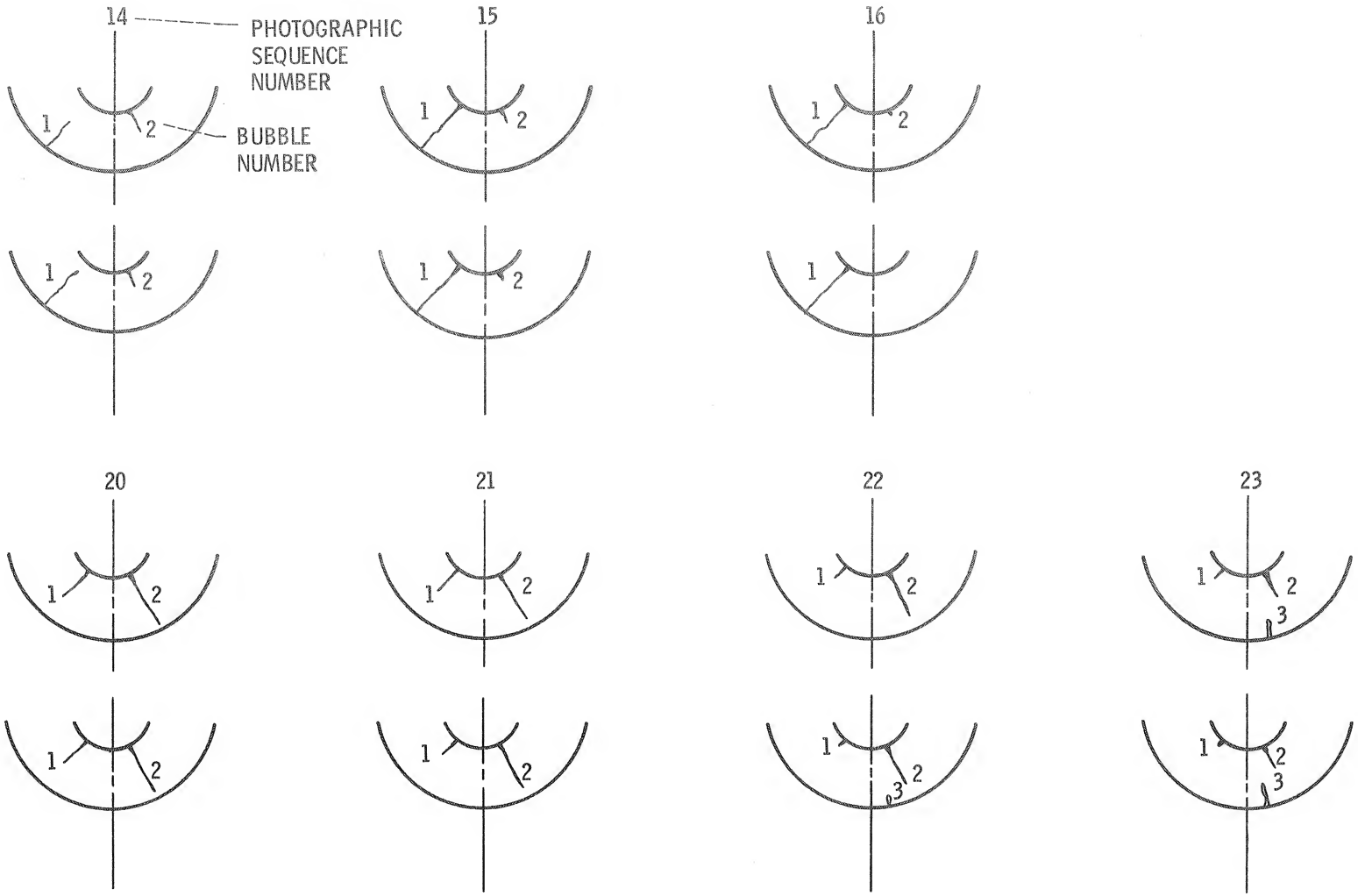
14
PHOTOGRAPHIC SEQUENCE NUMBER
BUBBLE NUMBER
15
16
20
21
22
23

Figure 9.

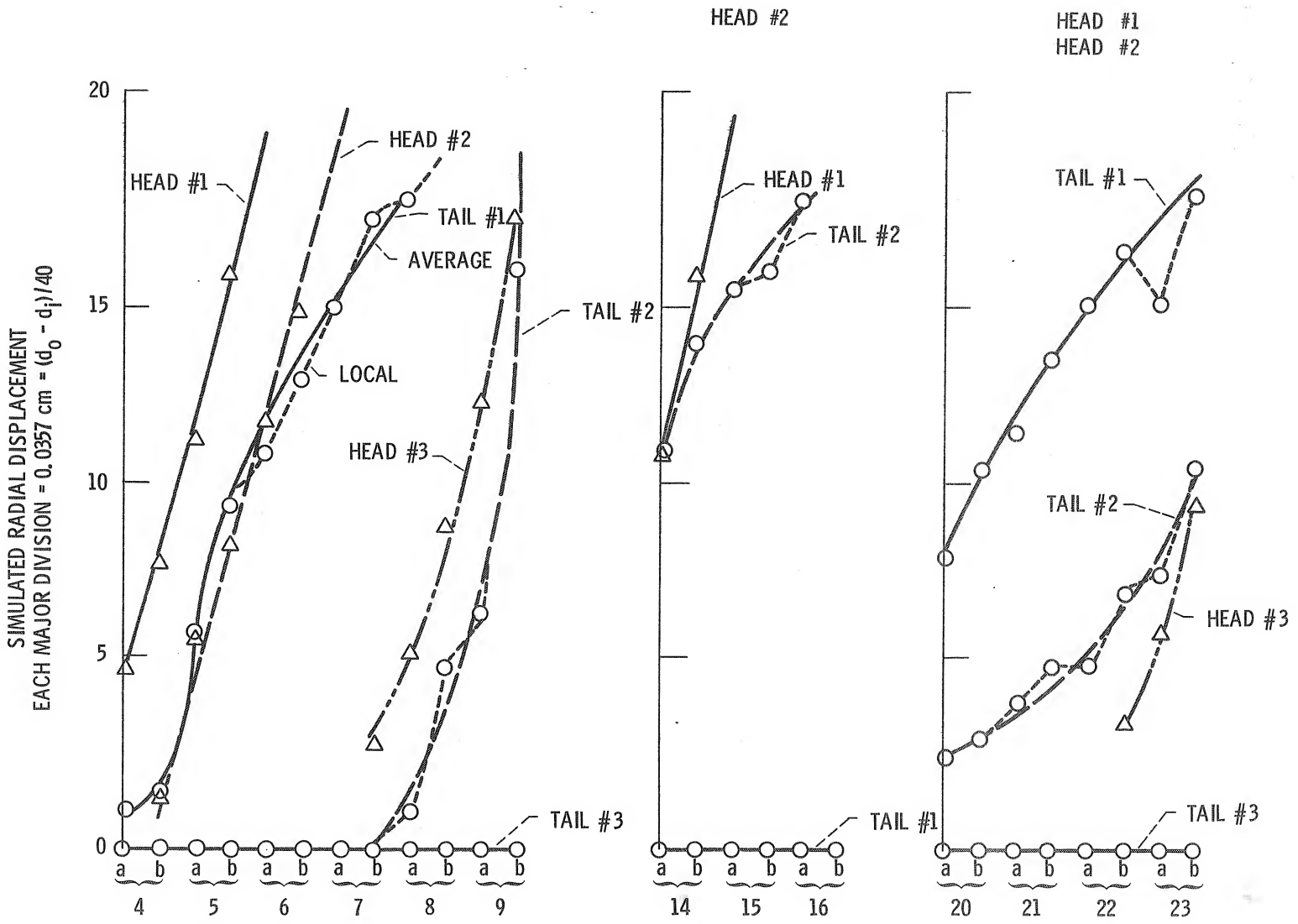

PHOTOGRAPHIC SEQUENCES (4-9), (14-16), (20-23) AND SIMULATED TIME SCALE; EACH MAJOR DIVISION = 1/18 200 sec = 55μ SEC

Figure 10. - Distance-time relations for selected bubble traverse shown in Figure 6.

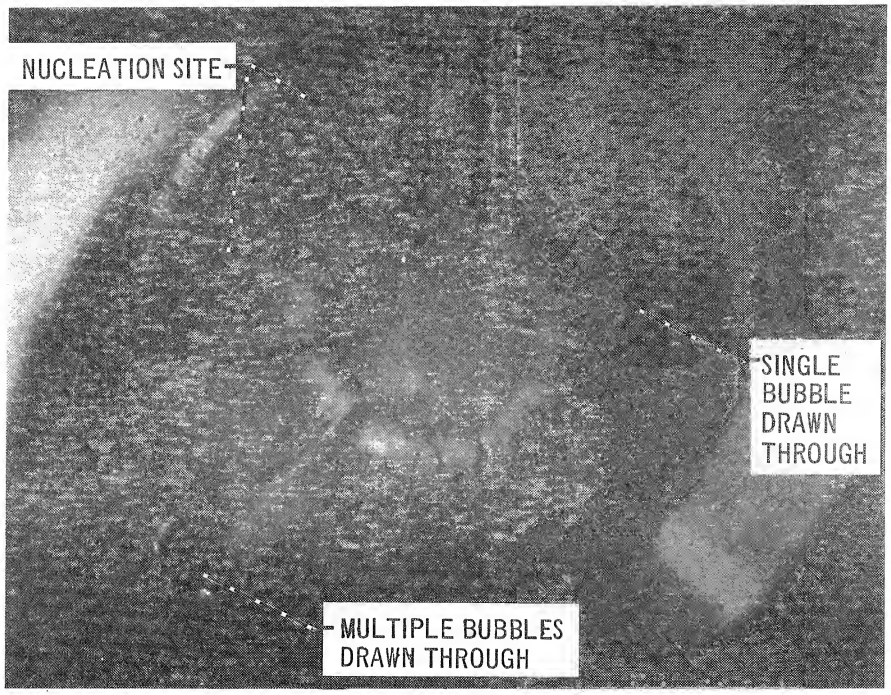

Figure 11. - Detailed picture of the bubble.

1. Report No.	2. Government Accession No.	3. Recipient's Catalog No.
NASA TM-83071		

4. Title and Subtitle	5. Report Date
ANALOGY BETWEEN FLUID CAVITATION AND FRACTURE MECHANICS	6. Performing Organization Code 505-33-52
7. Author(s) R. C. Hendricks, R. L. Mullen, and M. J. Braun	8. Performing Organization Report No. E-1519
9. Performing Organization Name and Address National Aeronautics and Space Administration Lewis Research Center Cleveland, Ohio 44135	10. Work Unit No.
	11. Contract or Grant No.
12. Sponsoring Agency Name and Address National Aeronautics and Space Administration Washington, D.C. 20546	13. Type of Report and Period Covered Technical Memorandum
	14. Sponsoring Agency Code

15. Supplementary Notes

R. C. Hendricks, NASA Lewis Research Center; R. L. Mullen, Case Western Reserve University, Dept. of Civil Engineering, Cleveland, Ohio 44106; and M. J. Braun, University of Akron, Dept. of Mechanical Engineering, Akron, Ohio 44325. Prepared for the Thermal Engineering Joint Conference cosponsored by the American Society of Mechanical Engineers and the Japan Society of Mechanical Engineers, Honolulu, Hawaii, March 20-24, 1983.

16. Abstract

When the stresses imposed on a fluid are sufficiently large, rupture or cavitation can occur. Such conditions can exist in many two-phase flow applications, such as the choked flows, which can occur in seals and bearings. Nonspherical bubbles with large aspect ratios have been observed in fluids under rapid acceleration and high shear fields. These bubbles are geometrically similar to fracture surface patterns (Griffith crack model) existing in solids. Analogies between crack growth in solid and fluid cavitation are proposed and supported by analysis and observation (photographs). Healing phenomena (void condensation), well accepted in fluid mechanics, have been observed in some polymers and hypothesized in solid mechanics. By drawing on the strengths of the theories of solid mechanics and cavitation, a more complete unified theory can be developed.

17. Key Words (Suggested by Author(s))	18. Distribution Statement
Cavitation; Fracture; Two-phase; Seals; Bearings; Tribology; Fluid mechanics; Fracture mechanics	Unclassified - unlimited STAR Category 34

19. Security Classif. (of this report)	20. Security Classif. (of this page)	21. No. of Pages	22. Price*
Unclassified	Unclassified		

* For sale by the National Technical Information Service, Springfield, Virginia 22161